

Understanding the cavitation and crazing behavior in the polymer nanocomposite by tuning shape and size of nanofiller

Huan Zhang^a, Ruibin Ma^b, Dandan Luo^b, Wen Xu^{a,**}, Yunfeng Zhao^a, Xiuying Zhao^{b,c,***}, Yangyang Gao^{b,c,*}, Liqun Zhang^{b,c,****}

^a Aerospace Research Institute of Materials and Processing Technology, Beijing, 100076, People's Republic of China

^b Key Laboratory of Beijing City on Preparation and Processing of Novel Polymer Materials, Beijing University of Chemical Technology, 10029, People's Republic of China

^c State Key Laboratory of Organic-Inorganic Composites, Beijing University of Chemical Technology, 10029, People's Republic of China

ARTICLE INFO

Keywords:

Cavitation and crazing
Nanofiller shape
Molecular simulation

ABSTRACT

It is very crucial to understand the fracture mechanism of the polymer nanocomposites (PNCs) on the molecular level. In this work, the effect of the shape and size of nanofillers on it has been investigated in details by adopting a coarse-grained molecular dynamics simulation. First, the fracture energy of PNCs is found to be much higher for rod fillers than for sheet fillers and sphere fillers. Then it is reduced with increasing the nanofiller size much faster for sphere fillers than for sheet fillers and rod fillers which results from their interface and network. To better understand it, the bond orientation degree is characterized which can reflect the elongation. By calculating the stress contribution of matrix chains and nanofillers, the stress borne by matrix chains gradually decreases with the increase of nanofiller size for sphere fillers and sheet fillers while it is nearly same for rod fillers. In addition, the stress borne by sphere filler is gradually reduced with the nanofiller size while it borne by rod fillers and sheet fillers rises. The former is closely related to the number of the interfacial beads which bear the high stress while the latter is attributed to the stress contribution by the bond/angle energy. Furthermore, the number of voids is quantified which first increases and then decreases with the strain which reflects the generation and coalescence of voids. Meanwhile, the voids prefer to nucleate in the matrix which is a weak region at the strong interfacial interaction. Last, the maximum number of voids gradually increases with the nanofiller size for sphere fillers and sheet fillers while it is nearly unchanged for rod fillers which is consistent with the matrix region. In summary, this work could provide a further understanding how the nanofiller shape affects the fracture properties of PNCs.

1. Introduction

Filled polymer nanocomposites (PNCs) are ubiquitous engineering polymers demonstrating the high tensile strength, deformability and toughness [1–3]. The remarkable reinforcement can be realized by adding a large amount of nanofillers into the matrix which however gives rise to a complex mechanical behavior. The mechanical property of PNCs correlates intimately with its structural evolution during the

deformation which will be influenced by many parameters (such as the size, volume fraction, grafting modification of nanofillers [4,5], the polymer-nanofiller interaction [6,7] and so on). Although this structural evolution plays a key role in determining the mechanical properties, a fundamental understanding of the fracture mechanism on a molecular scale has not been achieved yet.

Crazing is a unique mode of failure for PNCs during the tensile deformation where a strong dilatational component induces a rapid

* Corresponding authors. Key Laboratory of Beijing City on Preparation and Processing of Novel Polymer Materials, Beijing University of Chemical Technology, 10029, People's Republic of China.

** Corresponding author.

*** Corresponding authors. Key Laboratory of Beijing City on Preparation and Processing of Novel Polymer Materials, Beijing University of Chemical Technology, 10029, People's Republic of China.

**** Corresponding author. Key Laboratory of Beijing City on Preparation and Processing of Novel Polymer Materials, Beijing University of Chemical Technology, 10029, People's Republic of China.

E-mail addresses: zhangh@iccas.ac.cn (X. Zhao), gaoyy@mail.buct.edu.cn (Y. Gao), zhaoxy@mail.buct.edu.cn (L. Zhang).

<https://doi.org/10.1016/j.polymer.2019.122103>

Received 4 November 2019; Received in revised form 16 December 2019; Accepted 19 December 2019

Available online 24 December 2019

0032-3861/© 2020 Elsevier Ltd. All rights reserved.

volume gain before failure. During the fracture process, nanovoids first appear and then grow into a microcavity which finally induces the breakage of materials [8,9]. Accompanied by it, the slippage and extension of polymer chains happen. This process will dissipate a large amount of energy which is very important for their use in load-bearing applications. Thus, the nucleation and growth of nanovoids are key steps in uncovering the fracture mechanism. Recently, intensive studies have been devoted to address this fundamental question with the aim of realizing better performance. For instances, the development of crazes is related to the kinetics of the local plastic deformation by adopting constitutive equations [10]. Three stages of the rearrangement process of fillers are revealed during craze formation and propagation in glassy PNCs [11]. The small-angle X-ray scattering (SAXS) is a powerful tool for detecting nanovoids in the matrix during the fracture process. Currently, Zhang et al. [12–15] explored the formation of nanovoids in the carbon black filled styrene-butadiene rubber for the first time. However, the size of the detected nanovoids ranges from 20 to 30 nm which is larger than that (less than 10 nm) of the most initial ones. Thus, the nucleation and the evolution process of nanovoids is very difficult to be accurately recorded in experiments. With the development of the computer technology, molecular dynamics (MD) simulation becomes very powerful in characterizing the microstructural evolution during the tensile deformation which provides the access to elucidate the fracture mechanism at the molecular level. By adopting MD method, the initial voids are reported to preferentially form in the region of high chain ends density [16] or the low elastic modulus [17]. For example, nanovoids appear in the matrix for the attractive polymer-filler interaction while they are created at their interface for the repulsive interaction [18]. In addition, the void formation and the failure in rods filled PNCs can be predicted by the voronoi volume [19]. Meanwhile, nanorods incorporated into the crazes rapidly orient themselves to match the direction of the polymer fibrils while they in bulk regions remain randomly oriented. Moreover, the broad distribution of the tensile force in glassy polymers is reported to imply the fibril breakdown and the ultimate strength of craze [20]. During the fracture process, the amounts of the dissipated energy can be roughly divided into three types of rapid motion: cavitation, plastic yield and bridge rupture [21]. By investigating the failure modes in glassy polymer films confined between two solid surfaces, three modes of failures are revealed (few cavities, many single bridges, one large bridge) which depends on the degree of confinement [22]. By tuning the polymer chain length, the failure mode of crazes changes from disentanglement to scission. Meanwhile, the breakdown through scission is governed by large stress fluctuations [9]. In a regime of strong polymer-filler interactions, the small fillers are the most effective at reinforcing the matrix by surrounding the polymer chains [23]. Gersappe attributed it to the high mobility of small fillers which can dissipate the deformation energy via an improved release of local tension [24]. However, in conflict with it, the reinforcement is nearly independent of the mass of fillers which will affect its mobility [25]. There is no consistent conclusion of the role of the filler dynamics on the reinforcement mechanism. In addition, the high cross-linking density can inhibit the growth of cavities which enhances the brittle behavior. In the grafted fillers filled PNCs, the optimal fracture property is realized at the mediated grafting density [26,27]. Furthermore, by modifying the interaction strength between the nanoparticles and the inner block of diblock copolymers, the cavitation process and strain-softening behavior of glassy PNCs can be largely manipulated [28].

Based on the above works, even though the effect of the nanofiller shape on the dynamics property and the fracture property has been investigated [25,29,30], a fundamental understanding of the fracture mechanism has not been clearly identified yet. In experiments there are lots of the factors which affect the fracture behavior which is very difficult to isolate the effect of the nanofiller shape on it [4,31,32]. To uncover this fracture mechanism of PNC with different shapes and sizes, it is very important to understand the nucleation and evolution process of voids during the fracture process which has not been investigated to

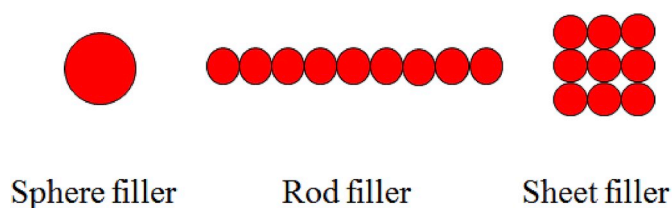


Fig. 1. Cartoons of nanofillers with three kinds of shapes: sphere filler, rod filler and sheet filler.

our knowledge. In this work, we adopted a coarse-grain model to investigate their fracture behavior at the molecular level by tuning the size and shape of nanofillers. The change of the microstructure inside the system is analyzed carefully in details with respect to the strain which presents a clear understanding of the fracture mechanism. We focused on the following two questions: (1) Depending on the size and shape of nanofillers, how the matrix chains and nanofillers contribute to the total stress respectively and the inner mechanism. (2) Where the nucleation of voids preferentially occurs and what the evolution process of voids is during the tensile process.

2. Simulation models and methods

To perform the simulation work, we adopted the classical coarse-grained model of the nanofillers filled PNCs with different shapes and sizes. The bead-spring model [33] is adopted to simulate the polymer chain which consists of thirty beads. Each system contains 800 chains. As shown in Fig. 1, three kinds of nanofiller shapes are considered in this work, namely sphere filler, rod filler and sheet filler. It is noted that the diameter and the mass of each polymer bead are denoted by the symbols σ and m respectively. When mapping the coarse-grained model to real polymers, the interaction parameter ϵ is set to be about 2.5–4.0 kJ mol⁻¹ for different polymers [33,34]. Meanwhile, one polymer bead with a diameter 1σ is roughly about 1 nm which roughly corresponds to 3–5 repeating units of polybutadiene [35–37]. Although the chains are rather short compared to real chains, they can display the static and dynamic characteristic behavior of long chains. In total, our simulation falls within a parameter rage in experiments which can capture the typical polymer system.

The expanded Lennard-Jones (LJ) potential is employed to describe the nonbonded interactions between all beads interactions [33], as follows

$$U_{ij}(r) = \begin{cases} 4\epsilon_{ij} \left[\left(\frac{\sigma}{r-\Delta} \right)^{12} - \left(\frac{\sigma}{r-\Delta} \right)^6 \right] + C & r - \Delta < r_{cutoff} \\ 0 & r - \Delta \geq r_{cutoff} \end{cases} \quad (1)$$

where C is a constant to guarantee that the potential energy is continuous everywhere. r is the distance between two interaction sites. r_{cutoff} stands for the distance $(r - \Delta)$ at which the interaction is truncated and shifted so that the energy is zero. The interaction range is offset by Δ to account for the excluded volume effect for two interaction sites. Here, Δ is chosen to be $(D_1 + D_2)/2 - \sigma$ where D_1 and D_2 are diameters of two interaction sites. The polymer-polymer interaction parameter and its cutoff distance are $\epsilon_{pp} = 1.0$ and $r_{pp} = 2.5$ respectively. The polymer-filler interaction parameter and its cutoff distance are $\epsilon_{pn} = 3.0$ and $r_{pn} = 2.5$ which aims to model a long-ranged attractive attraction. The filler-filler interaction parameter is $\epsilon_{nn} = 1.0$ with its cutoff distance $r_{nn} = 2.5$. It is noted that ϵ is the pair interaction energy scale and σ defines the length scale of our model. Since it is not our aim to study a specific polymer chain, all parameters are simplified by setting ϵ and σ equal to unit. Thus, all the simulated quantities are dimensionless.

The stiff harmonic potential is used to describe the bond energy between the adjacent beads in the polymer chain, rod filler and sheet filler, given by

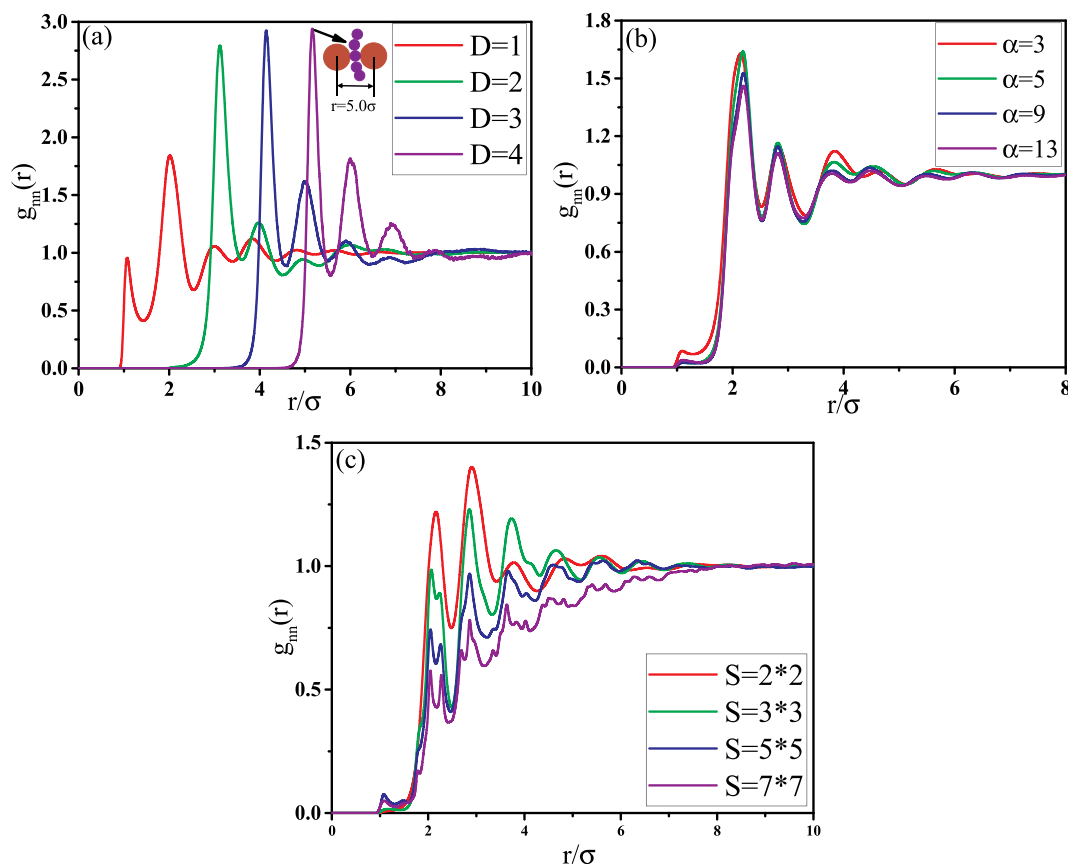


Fig. 2. RDF of (a) sphere fillers, (b) rod fillers and (c) sheet fillers for different sizes. ($T^* = 1.0$, $\phi = 10.3\%$).

$$U_{bond} = K(r - r_0)^2 \quad (2)$$

where K is equal to $1000 (\epsilon/\sigma^2)$ and r_0 is set to be 1σ . These parameters can guarantee a certain stiffness of the bonds while avoiding high-frequency modes and chain crossing. Meanwhile, it is reported that the harmonic potential is proved to be efficient in modeling polymer systems [38,39].

Following the work [29,30], the angle energy of the rod filler and the sheet filler is enforced by a bending potential, given by

$$U_{angle} = K(\theta - \theta_0)^2 \quad (3)$$

where θ is the bending angle formed by three beads, K is set to be 1000. θ_0 are set to be 180° for the rod filler and 90° or 180° for the sheet filler respectively. This setting can be sure to obtain the nanofillers with different shapes.

After determining the force field parameters, the simulations are started from a nonoverlapped configuration of all the polymers and the nanofillers into a large box [40–42]. Then, the simulation system is compressed for 20000τ under the NPT ensemble where the temperature and the pressure are fixed at $T^* = 1.0$ and $P^* = 0.0$ respectively by using the Nose-Hoover temperature thermostat and pressure barostat 4. Further equilibration is performed under the NVT ensemble with $T^* = 1.0$ which is above the glass transition temperature T_g (≈ 0.5) for 20000τ . It has been checked that each chain has moved at least $2R_g$. During the simulation process, three-dimensional periodic boundary conditions are adopted to eliminate edge effects. The equations of motion are integrated by using the velocity-Verlet algorithm with a time step $\delta t = 0.001\tau$ where τ is the LJ time ($\tau = \sigma\sqrt{m/\epsilon}$). The equilibrium number density of polymer beads is nearly 0.85 which corresponds to the density of polymer melts. After that, the structure and dynamics data are collected for the structural and dynamical analysis. At present, there

exist two typical approaches to simulate the fracture behavior of PNCs. For the first method, the polymer chains are clamped by using two rigid walls. The polymer failure is induced by the pure tensile strain by fixing the bottom wall and moving the top wall away from the bottom one. At this case, periodic boundary conditions are applied in the lateral two directions of the walls [22,25]. For the second method, the tri-axial deformation is exerted on the polymer to induce the failure. The length of the simulation box in one direction is extended while it in other two dimensions is held fixed which results in a positive effective stress in all directions [19,43]. In this case, the rigid walls are removed and periodic boundary conditions are applied in three directions. We adopted the second method to simulate the occurrence of the voids in this work. The strain rate is set to be $\alpha = 0.01/\tau$ which is adopted by Gao et al. [44]. It is noted that the strain rate (10^9 s^{-1}) is much larger than that in experiments. The average stress-strain curve is calculated by independently deforming each system along x, y and z directions respectively. All simulations have been performed by using the large scale atomic/molecular massively parallel simulator (LAMMPS) [45]. As stated in the introduction, the nucleation and evolution process of voids is a key factor which determines the fracture properties of PNCs. Thus, we first introduced the definition of voids which is a prerequisite to uncover the fracture mechanism. The simulation box is first divided into the small cubic sub-cells of size δ . After that, whether the polymer beads or nanofiller beads are within these small sub-cells will be checked which depends on their positions. If there are no beads within sub-cells, they are considered to be unoccupied which acts as voids. Otherwise, they are occupied by beads which are not belong to voids. At this moment the position and the number of sub-cells are obtained. Furthermore, the unoccupied sub-cells are considered to belong to the same void if they share a common face (namely they are neighbors). Finally the number of voids is obtained from these analysis. For the size δ of the sub-cell, it is chosen to be about 1.5σ in this work to meet that there is no voids in the

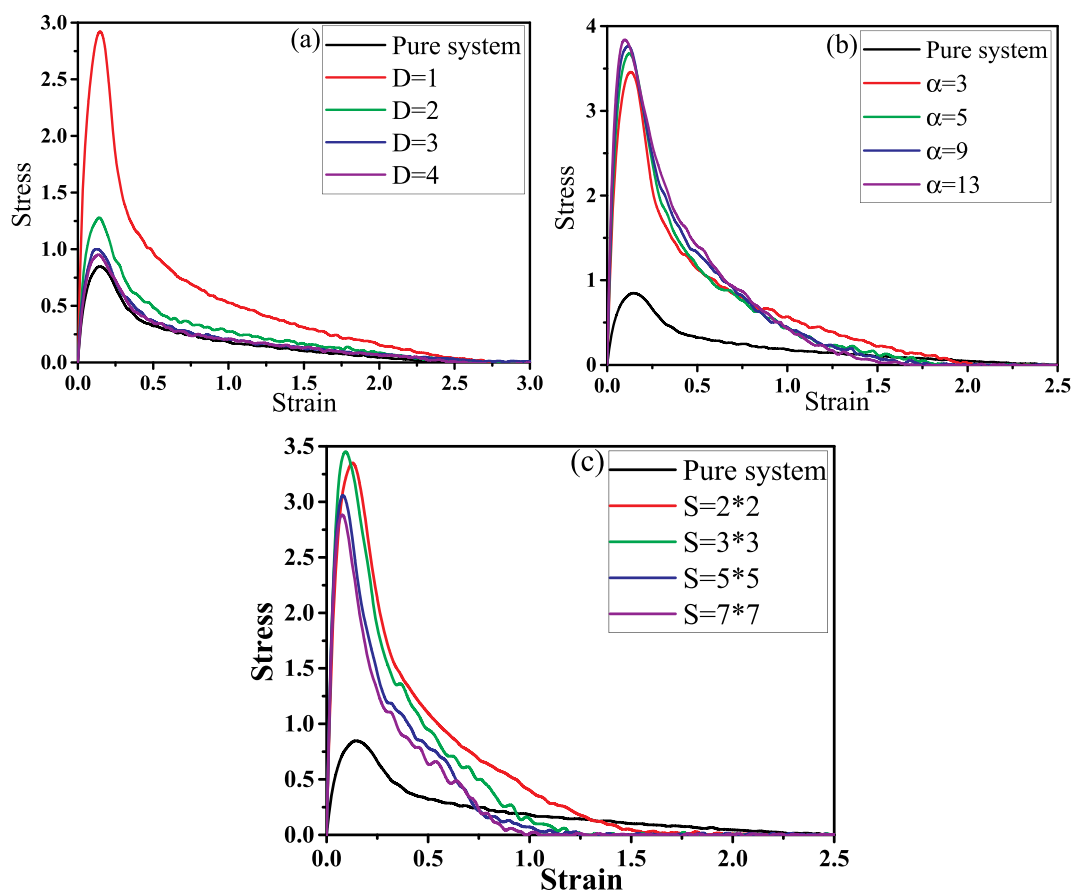


Fig. 3. The stress-strain curves for (a) sphere fillers, (b) rod fillers or (c) sheet fillers with different sizes. ($T^* = 1.0$).

unstrained system. Our size of the sub-void is comparable with that of a simulated bead which is adopted in the previously published work [16].

3. Results and discussion

3.1. Fracture property

In experiments, it is necessary to add the nanofillers into the polymer matrix for reinforcing the mechanical property [4,31,32]. The commonly used nanofillers has different shapes and sizes such as carbon black, silica, carbon nanotube, graphene and so on. Thus, in this part we mainly investigated the effect of the shape and size of nanofillers on the fracture properties of PNCs. Before discussing the fracture behavior of PNCs, it is useful to characterize the dispersion state of nanofillers by calculating the inter-nanofiller radial distribution function (RDF) in Fig. 2. It is noted that the volume fraction of nanofiller is about $\phi = 10.3\%$ and the polymer-filler interaction ϵ_{pn} is set to be 3.0 for each system. The details of the simulated systems for different shapes and sizes of nanofiller can be referred to Table SI. From Fig. 2(a), the peak at $r = \text{diameter (D)}$ stands for the direct contact aggregation of sphere fillers while it at $r = D + 1$ reflects that sphere fillers aggregate sandwiched by one polymer layer. These two kinds of structures coexist for $D = 1\sigma$. Then the peaks are shifted to a large value with the increase of D. Meanwhile, the direct contact aggregation of sphere fillers disappears which is reflected by the inexistence of the peak at $r = D$. Sphere fillers mainly form the sandwiched structure via one polymer layer. Even though there appears a low peak at $r = 1\sigma$ in Fig. 2(b), the rod fillers aggregation is mainly bridged through one polymer layer which is proved by the high peak at $r = 2\sigma$. Meanwhile, the dispersion state of rod fillers is similar for different aspect ratio α . Then we tuned to the dispersion state of sheet fillers in Fig. 2(c). It presents that the height of

peaks is gradually reduced with the increase of the size (S) of sheet fillers. It is noted that the number of sheet fillers is reduced with increasing S which leads to the large distance between them. In total, the dispersion state of nanofillers is relatively uniform in the matrix which can be observed directly from the snapshots in Fig. S1. This can isolate the effect of the shape and size of nanofillers on the fracture property. Then, the tri-axial deformation is performed to characterize the fracture property and analyze the change of the microstructure within the system during the tensile process. First, the stress is calculated with respect to the strain for different systems in Fig. 3. It is found that the stress first increases linearly with the strain and then reaches the maximum value quickly. After that it gradually drops to zero. The transition strain at the maximum stress is about 0.10. It is noted that the evolution process of voids with the strain is directly related to the stress-strain behavior which is affected by the shape and size of nanofillers. To quantitatively analyze the fracture property, the maximum stress, the elongation (strain at stress = 0.0) and the fracture energy (area formed by stress-strain curves and the x axis) are calculated which are listed in Table SII. All the PNCs exhibit the reinforcement effect compared with the pure system. For sphere fillers in Fig. 3(a), the maximum stress gradually decreases with increasing the D while the elongation is nearly unchanged. Thus, it leads to the gradual decline of the fracture energy. For rod fillers in Fig. 3(b), the maximum stress exhibits a limited increase with increasing the aspect ratio α while the elongation is reduced. Interestingly, the fracture energy is similar for them. For sheet fillers in Fig. 3(c), the maximum stress first shows a weak increase and then decreases with increasing the S while the elongation gradually declines. As a result, the fracture energy is gradually reduced. In general, the interfacial polymer beads can help to build the polymer-filler network. To better characterize it, the number of the interfacial polymer beads (N_p) is calculated which is shown in Fig. S2(a). It is found that the N_p is

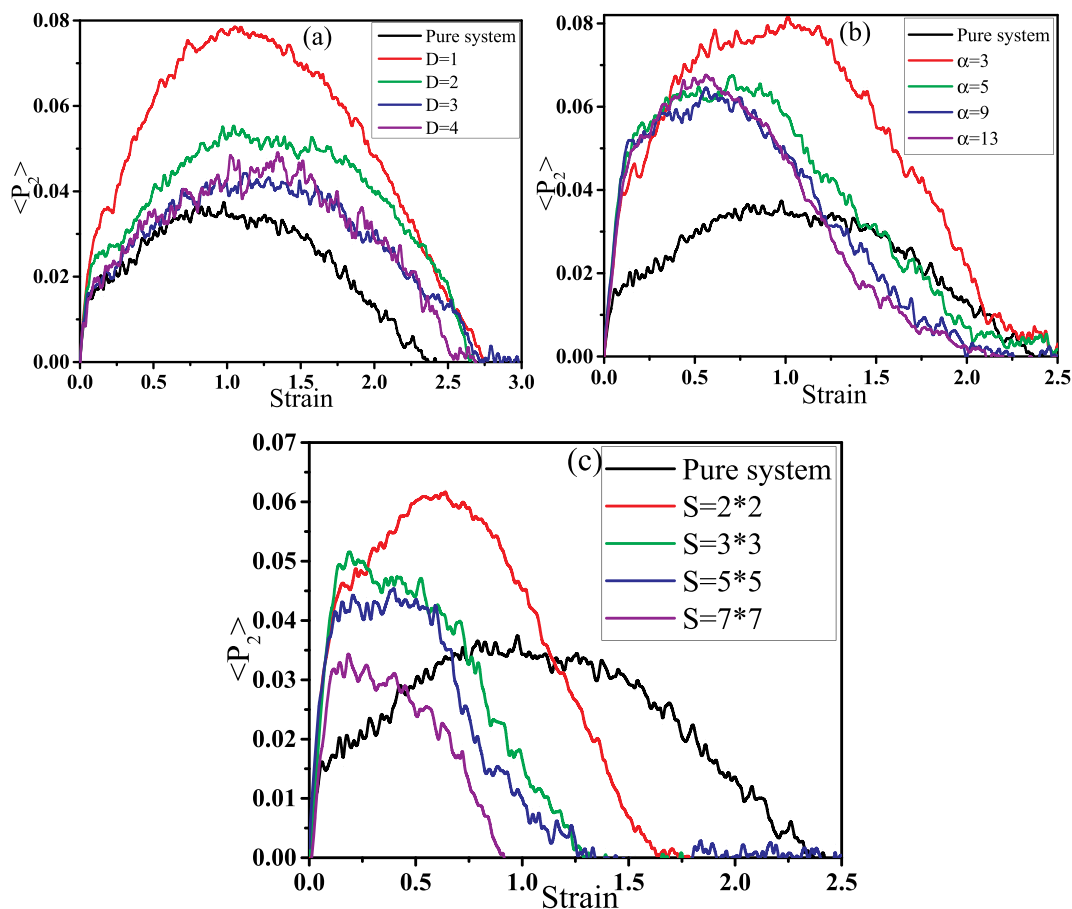


Fig. 4. The bond orientation degree $\langle P_2 \rangle$ of matrix chains for (a) sphere fillers, (b) rod fillers and (c) sheet fillers with different sizes. ($T^* = 1.0$).

gradually reduced with the increase of the nanofiller size. However, the falling rate is the largest for sphere fillers, the moderate for sheet fillers and the smallest for rod fillers. This results is consistent with the fracture energy. Then we intended to characterize the strength of the polymer-filler network which determines the maximum stress. This can be reflected by the diffusion coefficient of all the beads in Fig. S2(b). The low diffusion coefficient reflects the high strength of the polymer-filler network. It is found that the diffusion coefficient gradually increases with increasing D for sphere fillers while it decreases with increasing the α for rod fillers which is consistent with the maximum stress. Interestingly the diffusion coefficient first decreases and then increases with increasing the S for sheet fillers. Even though the N_p becomes less with increasing the nanofiller size, the mobility of the interfacial beads is also significantly reduced according to the previously published work [30,

46]. Because of these two competing effects in overall diffusion coefficients of chains, this actually explains how the maximum stress changes with the nanofiller size for different shapes. To further understand the fracture property, the bond orientation degree of matrix chains is characterized with respect to the strain which can reflect the elongation of PNCs. It is noted that the second-order Legendre polynomials $\langle P_2 \rangle$ is used to denote the bond orientation degree which is defined as $(3\langle \cos^2 \theta \rangle - 1)/2$. Here, θ denotes the angle between the bond vector and the tensile direction. Fig. 4 presents the dependence of the $\langle P_2 \rangle$ on the strain for different shapes and sizes of nanofiller. The bonds present the random orientation at the strain = 0.0 which leads to the $\langle P_2 \rangle = 0.0$. As the increase of strain, the $\langle P_2 \rangle$ first increases to the maximum value. Then it is gradually reduced to 0.0 for all systems. This indicates the initial extension and then contraction of matrix chains

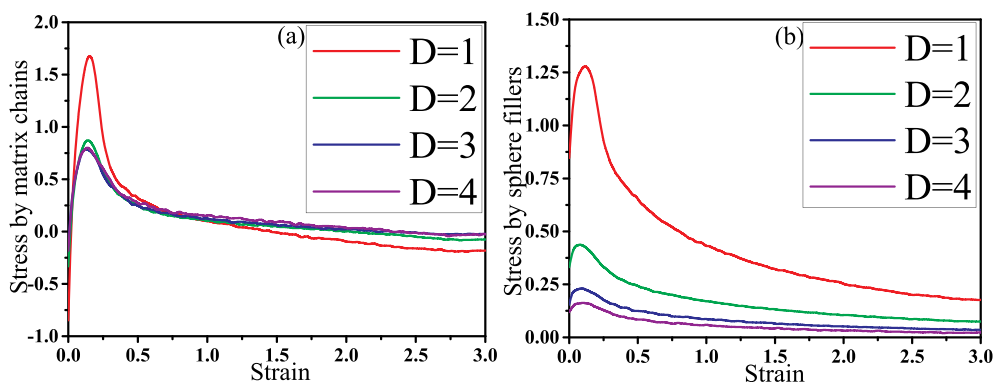


Fig. 5. The stress contributed by (a) matrix chains and (b) sphere fillers for different filler sizes D . ($T^* = 1.0$).

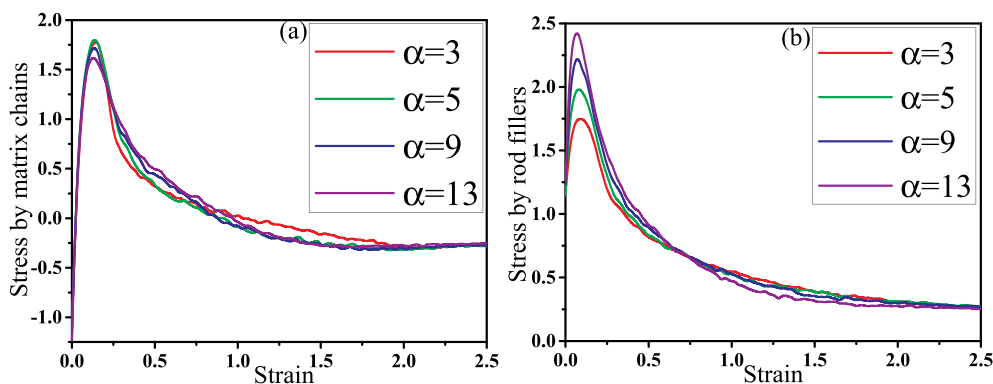


Fig. 6. The stress contributed by (a) matrix chains and (b) rod fillers for different nanofiller sizes α . ($T^* = 1.0$).

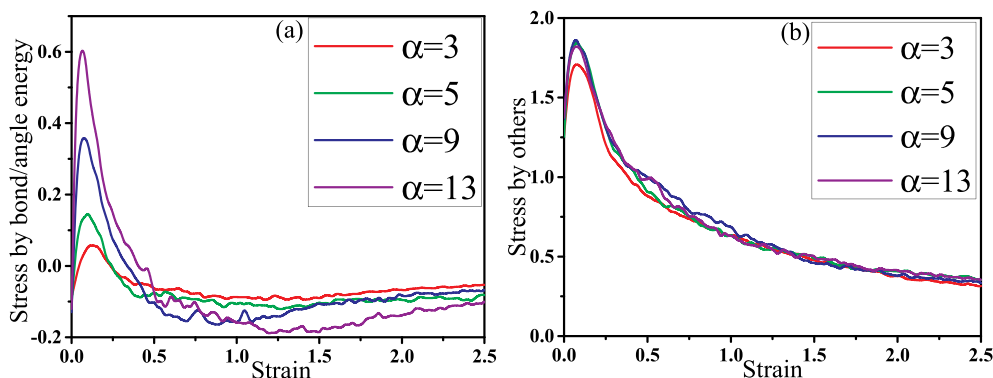


Fig. 7. The stress contributed by (a) bond/angle energy and (b) others for rod fillers with different filler sizes α . ($T^* = 1.0$).

during the tensile process which can reflect the fracture behavior. The trend of the strain at the $\langle P_2 \rangle = 0.0$ with the nanofiller size is similar to that of the elongation. Meanwhile, the mobility of the interfacial beads is reduced from sphere fillers, rod filler to sheet fillers [30] which leads to more stress concentration on the polymer-filler interface. This heterogeneous stress distribution will reduce the elongation of PNCs especially for sheet fillers. In total, the $\langle P_2 \rangle$ is less than 0.08 which has a limited effect on the stress-strain behavior. Then, to further understand how the shape and size of nanofiller influence the fracture property, we quantified the contribution of matrix chains and nanofillers to the total stress, respectively. For sphere fillers in Fig. 5, it is found that the stress contribution of both the matrix chains and sphere fillers is gradually reduced with increasing the D. On one hand, the number of the interfacial beads is gradually reduced with increasing the D in Fig. S2(a) which bear the high stress at the strong interfacial interaction. Thus, it reduces the stress contributed by matrix chains. On the other hand, the

stress transfers from matrix chains to sphere fillers via the interface. However, the interface area of big sphere fillers is less than that of small sphere fillers at the fixed concentration which reduces the stress contributed by sphere fillers. For rod fillers in Fig. 6, the stress contribution of matrix chains shows a very weak decrease with increasing the α while it of rod fillers is gradually enhanced. As shown in Fig. S2(a), the number of the interfacial beads exhibit a very limited decrease with the α which is consistent with the stress contributed by matrix chains. In addition, it is noted that the interface area is a little reduced with the increase of α which seems to contradict with their stress contribution. To further understand it, the stress contribution of the bond/angle energy and others is quantified for rod fillers in Fig. 7. It is interesting to find that the stress contribution of the bond/angle energy is enhanced while it of others is nearly unchanged with the increase of the α . This indicates that besides the polymer-filler interface, the nanofiller structure also affects their stress contribution during the tensile process. For sheet

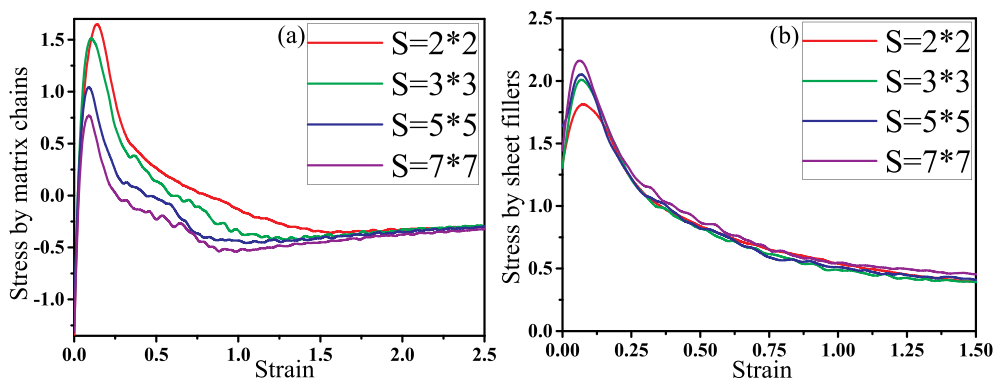


Fig. 8. The stress contributed by (a) matrix chains and (b) sheet fillers for different filler sizes S. ($T^* = 1.0$).

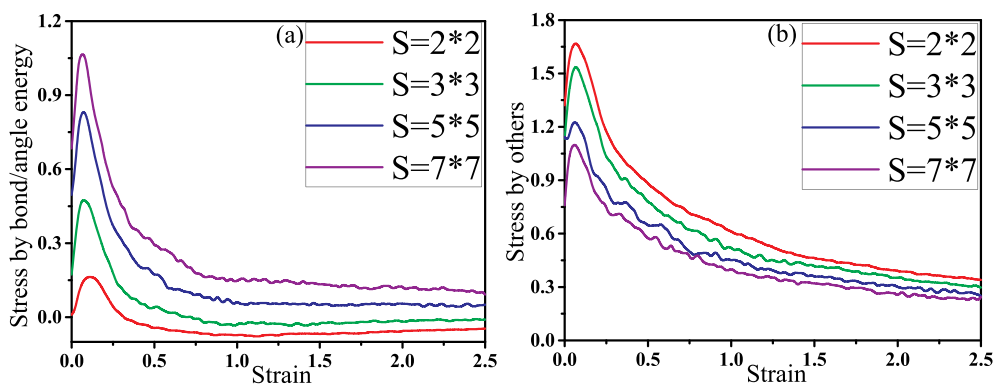


Fig. 9. The stress contributed by (a) bond/angle energy and (b) others for sheet fillers with different filler sizes S . ($T^* = 1.0$).

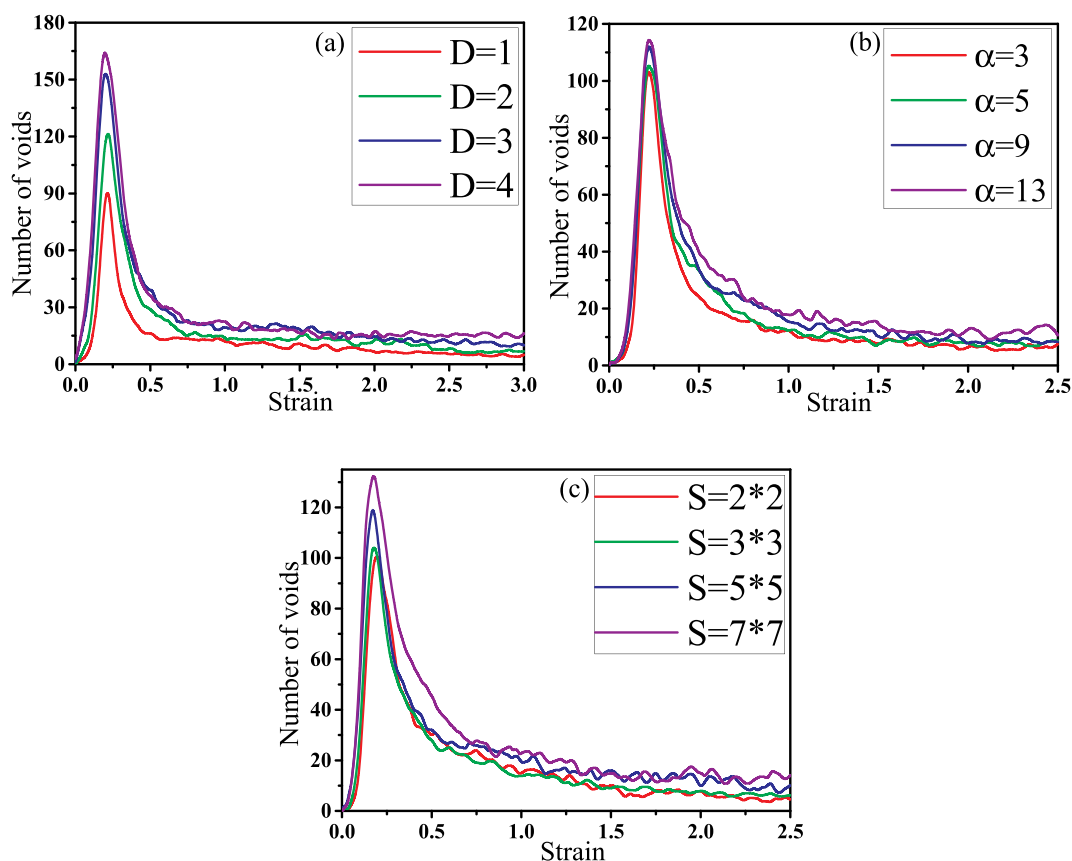


Fig. 10. The number of voids as a function of the strain for (a) sphere fillers, (b) rod filler and (c) sheet filler with different sizes. ($T^* = 1.0$).

fillers in Fig. 8, the stress contribution of matrix chains exhibits a continuous decrease with increasing the S while it of sheet filler is gradually enhanced. The reduced stress contribution of matrix chains is attributed to the less interfacial polymer beads for the high S in Fig. S2 (a). Similar to rod fillers, the stress by sheet fillers increases with their size which is attributed to more stress contribution by the bond/angle energy in Fig. 9(a). However, the stress contribution by others is also reduced with the S which is related to the small polymer-filler interface. In addition, it is noted that one filler with larger size bears more stress which is shown in Fig. S3. This is attributed to more interfacial beads surrounding one big filler compared with surrounding one small filler. Therefore, both the number of the interfacial beads (namely the polymer-filler interface) and the nanofiller structure determine the fracture property of PNCs which depends on their shape and size.

Last we will analyze the nucleation and evolution process of voids

during the fracture process which is a key parameter to gain more insight in the fracture behavior. The definition of voids can be referred to section 2. The change of the number of voids with the strain has been characterized for different shapes and sizes of nanofillers in Fig. 10. There are no voids at strain = 0.0 for all systems. Then some single voids appear with the increase of the strain (< 0.10) which is reflected by the maximum void size equal to 1 or 2 (not shown here). This indicates that there are one or two sub-cells within each void. Furthermore, there small voids gradually coalesce into large voids at the strain > 0.10 . This transition strain (≈ 0.10) is roughly consistent with that at the maximum stress in Fig. 2 which reflects that the small voids are isolated before the maximum stress. However, when the small voids are met each other to form a large one the stress begins to decrease. Then the number of the voids reaches the maximum value with the strain. When the generation rate of new voids is less than the coalescent rate, the number of voids

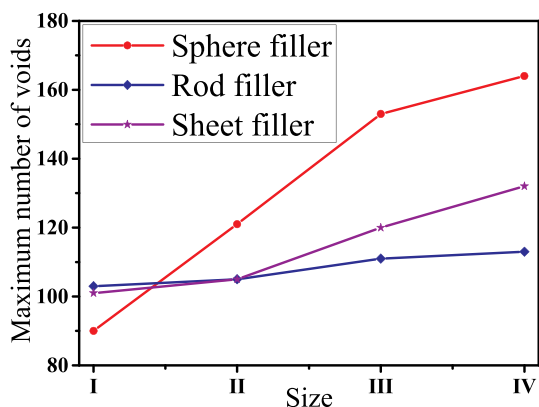


Fig. 11. The maximum number of voids for different shapes and sizes of nanofiller. ($T^* = 1.0$).

begins to decline with further increasing the strain. Finally, the percolated voids which spans the system induces the fracture of PNCs. Meanwhile, the maximum number of voids is recorded for different shapes and sizes of nanofillers in Fig. 11. It is found that the maximum number of voids gradually increases with the nanofiller size. However, the rising slope is the largest for sphere fillers, the moderate for sheet fillers and the smallest for rod fillers. This result is actually contrary to the interfacial polymer beads N_p in Fig. S2(a). To better understand it, we probed the positions where the nucleation of voids occurs. If the initial single voids can “meet” the nanofiller beads within the surface-surface distance $\approx 1.0\sigma$, these initial single voids are considered to generate at the polymer-filler interface. Otherwise, they generate in the matrix. In general, the initial voids are formed in the local weak regions rather than all regions. Meanwhile, the polymer-filler interface is considered to be the strong region than the matrix at the attractive interfacial interaction. To prove it, two systems are chosen ($D = 4$ and $S = 7 \times 7$) because they own a large matrix region compared with others. The ratio of voids which generate in the matrix to the total voids is about 94% for $D = 4$ and 85% for $S = 7 \times 7$. Thus, the nucleation of voids upon deformation occurs preferentially in the matrix region. In addition, the matrix region gradually increases with increasing the nanofiller size which thus improves the maximum number of voids. Last, to observe the voids during the tensile process, the snapshots corresponding to some

typical strains are shown in Fig. 12 for sphere fillers ($D = 1$), rod fillers ($\alpha = 13$) and sheet fillers ($S = 7 \times 7$) respectively. This can further help to understand the evolution process of voids.

Currently, the fracture property of PNCs has been investigated which depends on various factors such as the shape, size and concentration of fillers, the polymer-filler interaction and so on. [4], [31], [32], [47–49] It is reported [25], [29] that rod fillers can better reinforce the PNCs than sphere fillers and sheet fillers which is consistent with our results. Furthermore, Zhang et al. [12–15] adopted the SAXS method to explore the formation of nanovoids in the carbon black filled styrene-butadiene rubber for the first time. The void volume fractions are determined from the scattering invariant and the size of the detected nanovoids ranges from 20 to 30 nm. However, the most initial nanovoids with sizes less than 10 nm can not be detected. Meanwhile, such estimations are considered to be phenomenological because a large increase in scattering intensity near the primary beam is rather an indication of voids than a detection. Thus, the evolution process of nanovoids is very difficult to be accurately recorded. It is noted that our simulation describes a common polymer system which (nanoscale) are not on the same scale as experiments because the sample size is much smaller in simulation than in experiments. The chemical properties of nanofillers are not completely same in experiments. However, they are same for nanofillers in the simulation which can better isolate the effect of the nanofiller shape on the fracture behavior. Furthermore, the surface modification of nanofillers is adopted to improve the compatibility with the polymer matrix because of their self-attractive interaction in experiments. However, it is not enough to avoid their aggregation. Thus external fields (such as the shear field, tensile field and so on) are used to break the aggregation down. However, nanofillers will aggregate again when the external fields are removed. Thus, the dispersion state of nanofillers is not in the thermodynamic equilibrium state while they reach the thermodynamic equilibrium in the simulation. As a result, the dispersion state of nanofiller in the simulation is not completely same to that in experiments. Thus quantitative comparison between the experiments and our simulation is difficult. In our simulation, by analyzing the stress contribution of different components and the evolution process of initial nanovoids, this work gives a clear understanding on the fracture behavior of PNCs with different shapes and sizes of nanofiller.

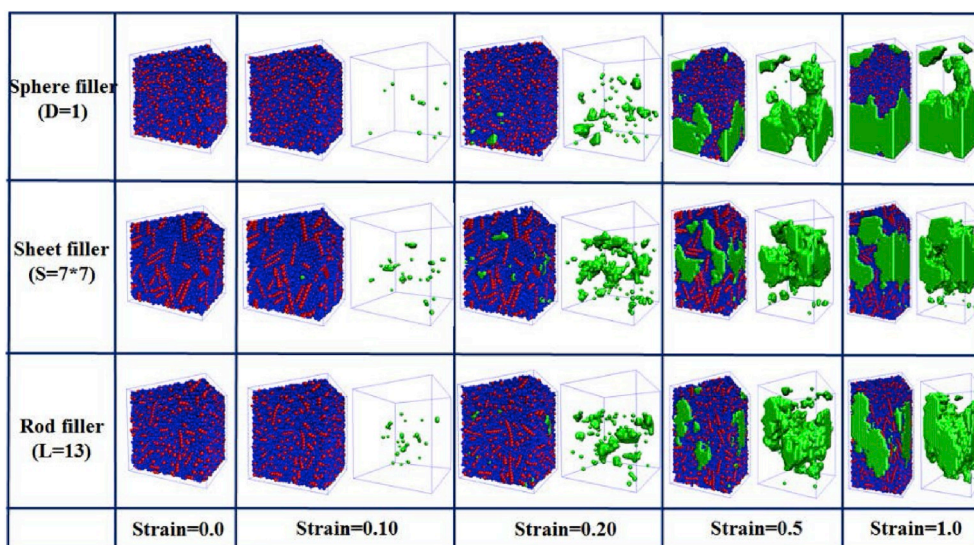


Fig. 12. Snapshots of systems with different nanofiller shapes during the fracture process at some strains. The blue spheres denote the polymer beads, the red beads denote the nanofillers and the green spheres denote the voids. For better clarify, voids are shown in right side where polymer and nanofillers are omitted. ($T^* = 1.0$). (For interpretation of the references to colour in this figure legend, the reader is referred to the Web version of this article.)

4. Conclusions

In this work, we adopted the molecular dynamics simulation to investigate the effect of the shape and size of nanofillers on the fracture property of the polymer nanocomposites (PNCs). PNCs with rod fillers exhibits the higher fracture energy than those with sheet fillers and sphere fillers. Meanwhile, the fracture energy is reduced with increasing the nanofiller size much faster for sphere fillers than for sheet fillers and rod fillers which can be reasonably explained by the polymer-filler interface and the polymer-filler network. To better understand it, we first characterized the bond orientation degree with respect to the strain which can reflect the elongation for different systems. By analyzing the stress contribution of matrix chains and nanofillers, the stress borne by matrix chains gradually decreases with increasing the nanofiller size for sphere fillers and sheet fillers while it is nearly same for rod fillers which closely depends on the number of the interfacial beads. In addition, the stress borne by sphere fillers is gradually reduced with the nanofiller size while it borne by rod fillers and sheet fillers rises because of the stress contribution by their bond/angle energy. Consistent with the stress-strain curves, the number of voids first increases and then decreases with the strain because of the coalescence of small voids into large ones. Meanwhile, the nucleation of voids prefers to occur in the matrix which is a weak region. Last, the maximum number of voids gradually increases with increasing the nanofiller size for sphere fillers and sheet fillers while it is nearly unchanged for rod fillers which depends on the matrix region. In summary, this work could provide a fundamental understanding on the fracture mechanism of PNCs on the molecular level by tuning the nanofiller shape.

Author Contributions

Data curation, Formal analysis: Huan Zhang, Ruibin Ma. Investigation, Methodology: Huan Zhang, Dandan Luo, Xiuying Zhao, Yunfeng Zhao; Project administration, Funding acquisition: Wen Xu, Liqun Zhang; Supervision, Writing-original draft; Writing-review & editing: Yangyang Gao, Liqun Zhang, Wen Xu, Xiuying Zhao;

Declaration of interest statement

The authors declare no conflict of interests.

Acknowledgements

The authors acknowledge financial supports from the National Natural Science Foundation of China (21704003, 51673013), National 973 Basic Research Program of China 2015CB654700(2015CB654704), the Foundation for Innovative Research Groups of the NSF of China (51521062) and the start-up funding of Beijing University of Chemical Technology for excellent introduced talents (buctrc201710). The authors acknowledge the National Supercomputer Centers in Lvliang, Guangzhou and Shenzhen.

Appendix A. Supplementary data

Supplementary data to this article can be found online at <https://doi.org/10.1016/j.polymer.2019.122103>.

References

- [1] F. Deng, M. Ito, T. Noguchi, L. Wang, H. Ueki, K.-i. Niihara, Y.A. Kim, M. Endo, Q.-S. Zheng, *ACS Nano* 5 (2011) 3858–3866.
- [2] J.M. Clough, C. Creton, S.L. Craig, R.P. Sijbesma, *Adv. Funct. Mater.* 26 (2016) 9063–9074.
- [3] C. Declet-Perez, L.F. Francis, F.S. Bates, *ACS Macro Lett.* 2 (2013) 939–943.
- [4] M.A. Rafiee, J. Rafiee, I. Srivastava, Z. Wang, H. Song, Z.-Z. Yu, N. Koratkar, *Small* 6 (2010) 179–183.
- [5] M. Morits, T. Verho, J. Sorvari, V. Liljeström, M.A. Kostianinen, A.H. Gröschel, O. Ikkala, *Adv. Funct. Mater.* 27 (2017) 1605378.
- [6] B. Guo, Z. Tang, L. Zhang, *Prog. Polym. Sci.* 61 (2016) 29–66.
- [7] Z. Tang, J. Huang, B. Guo, L. Zhang, F. Liu, *Macromolecules* 49 (2016) 1781–1789.
- [8] J. Rottler, M.O. Robbins, *Physical Review E* 64 (2001), 051801.
- [9] J. Rottler, M.O. Robbins, *Physical Review E* 68 (2003), 011801.
- [10] R. Estevez, M.G.A. Tijssens, E.V.D. Giessen, *J. Mech. Phys. Solids* 48 (2000) 2585–2617.
- [11] J.Y. Lee, Q. Zhang, A. Todd Emrick, A.J. Crosby, *Macromolecules* 39 (2006) 7392–7396.
- [12] H. Zhang, A.K. Scholz, J. de Crevoisier, F. Vion-Loisel, G. Besnard, A. Hexemer, H. R. Brown, E.J. Kramer, C. Creton, *Macromolecules* 45 (2012) 1529–1543.
- [13] H. Zhang, A.K. Scholz, F. Vion-Loisel, Y. Merckel, M. Brieu, H. Brown, S. Roux, E. J. Kramer, C. Creton, *Macromolecules* 46 (2013) 900–913.
- [14] H. Zhang, A.K. Scholz, J. de Crevoisier, D. Berghezan, T. Narayanan, E.J. Kramer, C. Creton, *J. Polym. Sci. B Polym. Phys.* 53 (2015) 422–429.
- [15] H. Zhang, A.K. Scholz, Y. Merckel, M. Brieu, D. Berghezan, E.J. Kramer, C. Creton, *J. Polym. Sci. B Polym. Phys.* 51 (2013) 1125–1138.
- [16] B. Sixou, *Mol. Simul.* 33 (2007) 965–973.
- [17] A. Makke, M. Perez, J. Rottler, O. Lame, J.L. Barrat, *Macromol. Theory Simul.* 20 (2011) 826–836.
- [18] K. Hagita, H. Morita, H. Takano, *Polymer* 99 (2016) 368–375.
- [19] G.N. Toepperwein, J.J.D. Pablo, *Macromolecules* 44 (2011) 5498–5509.
- [20] J. Rottler, M.O. Robbins, *Phys. Rev. Lett.* 89 (2002) 195501.
- [21] M.O. Robbins, *Science* 271 (1996) 482–484.
- [22] V.A. Froltsov, M. Klüppel, G. Raos, *Physical Review E* 86 (2012), 041801.
- [23] A. Kutvonen, G. Rossi, T. Ala-Nissila, *Physical Review E* 85 (2012), 041803.
- [24] D. Gersappe, *Phys. Rev. Lett.* 89 (2002), 058301.
- [25] A. Kutvonen, G. Rossi, S.R. Puisto, N.K.J. Rostedt, T. Ala-Nissila, *J. Chem. Phys.* 137 (2012) 214901.
- [26] F. Hu, Y. Nie, F. Li, J. Liu, Y. Gao, W. Wang, L. Zhang, *Phys. Chem. Chem. Phys.* 21 (2019) 11320–11328.
- [27] R. Shi, H.-J. Qian, Z.-Y. Lu, *Phys. Chem. Chem. Phys.* 21 (2019) 7115–7126.
- [28] R. Shi, H.-J. Qian, Z.-Y. Lu, *Macromolecules* 52 (2019) 7353–7360.
- [29] S.T. Knauer, J.F. Douglas, F.W. Starr, *J. Polym. Sci. B Polym. Phys.* 45 (2007) 1882–1897.
- [30] Y. Gao, J. Liu, J. Shen, Y. Wu, L. Zhang, *Phys. Chem. Chem. Phys.* 16 (2014) 21372–21382.
- [31] S. Bhattacharyya, C. Sinturel, O. Bahloul, M.-L. Saboungi, S. Thomas, J.-P. Salvetat, *Carbon* 46 (2008) 1037–1045.
- [32] T.H. Zhou, W.H. Ruan, M.Z. Rong, M.Q. Zhang, Y.L. Mai, *Adv. Mater.* 19 (2007) 2667–2671.
- [33] K. Kremer, G.S. Grest, *J. Chem. Phys.* 92 (1990) 5057–5086.
- [34] P. Gao, H. Guo, *Phys. Chem. Chem. Phys.* 17 (2015) 31693–31706.
- [35] A. Ghanbari, T.V.M. Nodoro, F. Leroy, M. Rahimi, M.C. Böhm, F. Müller-Plathe, *Macromolecules* 45 (2012) 572–584.
- [36] M. Rahimi, I. Iriarte-Carretero, A. Ghanbari, M.C. Böhm, F. Müller-Plathe, *Nanotechnology* 23 (2012) 305702.
- [37] C. Svaneborg, H. A. Karimi-Varzaneh, N. Hojdis, F. Fleck and R. Everaers, 2018, arXiv:1808.03509v03502..
- [38] H. Chao, R.A. Riggleman, *Polymer* 54 (2013) 5222–5229.
- [39] G. Raos, M. Moreno, S. Elli, *Macromolecules* 39 (2006) 6744–6751.
- [40] X. Duan, H. Zhang, J. Liu, Y. Gao, X. Zhao, L. Zhang, *Polymer* 168 (2019) 138–145.
- [41] Y. Gao, F. Qu, W. Wang, F. Li, X. Zhao, L. Zhang, *Compos. Sci. Technol.* 176 (2019) 37–45.
- [42] Y. Gao, F. Hu, Y. Wu, J. Liu, L. Zhang, *Comput. Mater. Sci.* 142 (2018) 192–199.
- [43] R. Estevez, D. Long, *Model. Simul. Mater. Sci. Eng.* 19 (2011), 045004.
- [44] J. Gao, J.H. Weiner, *Macromolecules* 29 (1996) 6048–6055.
- [45] S. Plimpton, *J. Comput. Phys.* 117 (1995) 1–19.
- [46] H. Eslami, M. Rahimi, F. Müller-Plathe, *Macromolecules* 46 (2013) 8680–8692.
- [47] X. Cao, X. Zhou, G. Weng, *Polym. Adv. Technol.* 29 (2018) 1779–1787.
- [48] B. Zhong, Z. Jia, Y. Luo, D. Jia, F. Liu, *Polym. Test.* 58 (2017) 31–39.
- [49] S. Chatterjee, F. Nafezarefi, N.H. Tai, L. Schlagenhauf, F.A. Nüesch, B.T.T. Chu, *Carbon* 50 (2012) 5380–5386.